Advanced Materials

ADVANCED MATERIALS
www.advmat.de

RESEARCH ARTICLE OPEN ACCESS
Editor's Choice

Hydrogelation via Supramolecular Copolymerization of Structural Water within Adaptive Metal–Organic Fibers

Merlin R. Stühler[1,2] | Hesam Makki[3] | Tarek Hilal[2] | Debsena Chakraboty[1] | Mathias Dimde[2] | Kai Ludwig[2] | Rainer Haag[2] | Sabine Rosenfeldt[4,5] | Dorothee Silbernagl[6] | Andreas Schäfer[2] | Alex J. Plajer[1,4]

[1]Makromolekulare Chemie, Universität Bayreuth, Bayreuth, Germany | [2]Institut Für Chemie und Biochemie, Freie Universität Berlin, Berlin, Germany | [3]Department of Chemical Engineering, University of Bath, Bath, UK | [4]Bayrisches Polymer Institut (BPI), Universität Bayreuth, Bayreuth, Germany | [5]Physikalische Chemie I, Universität Bayreuth, Bayreuth, Germany | [6]Bundesanstalt für Materialforschung und -Prüfung (BAM), Berlin, Germany

Correspondence: Alex J. Plajer (alex.plajer@uni-bayreuth.de)

Received: 13 October 2025 | **Revised:** 23 December 2025 | **Accepted:** 12 January 2026

Keywords: DFT calculations | hydrogels | self-assembly | single particle analysis | supramolecular polymerization

ABSTRACT

Water is conventionally viewed as a disruptive solvent for supramolecular materials, destabilizing directional noncovalent interactions. Here, we report a metal–organic material in which water instead acts as a structural co-monomer driving the formation of supramolecular fibers. A zinc(II) bisphenoxyimine ("Salphen") complex featuring convergent hydrogen-bond acceptor sites assembles in bulk water into long, hollow nanofibers stabilized by confined structural water molecules. Single-particle analysis and density functional theory reveal tubular architectures in which intercalated water bridges the metal centers and defines a hydrophilic inner channel. The fibers form hydrogels with thermomechanical response, chemically triggerable disassembly and enable selective chiral recognition of amino acids via water-mediated molecular–to–supramolecular information transfer. In organic solvents, the water content can be used for control over supramolecular self-assembly and hence gelation and liquefaction. Our findings establish structural water as a design element for creating adaptive, chiral, and dynamically reconfigurable metal–organic materials, offering a new paradigm to unlock this sustainable building block in supramolecular materials design.

1 | Introduction

Self-assembly in aqueous environments underlies the formation of many complex architectures [1–5]. During this process, water is expelled from nonpolar surfaces, which is commonly termed the hydrophobic effect. However, in some biological assemblies, not all water is excluded, and a distinct class of structural water molecules is frequently retained within assemblies, where they form persistent, directional hydrogen bonds that even translate homochiral information [6–9]. In contrast, in synthetic supramolecular assemblies and materials, water is typically deliberately excluded rather than incorporated during the assembly (Figure 1a) [10–18]. For example, hydrogen bonding motifs are often even shielded with hydrophobic groups to avoid solvation of the directional interactions that enable supramolecular polymerization in water [19–22]. Elsewhere, water molecules can reside and diffuse within the hydrophobic regions of aqueous assemblies or be confined in hydrophilic compartments such as coacervates that self-assemble in water. However, in these cases, water is unlikely to play a central architectural role in which its 3D requirements for structure and bonding dictate the morphology of the self-assembled nanostructure [23–25]. As a result, the idea

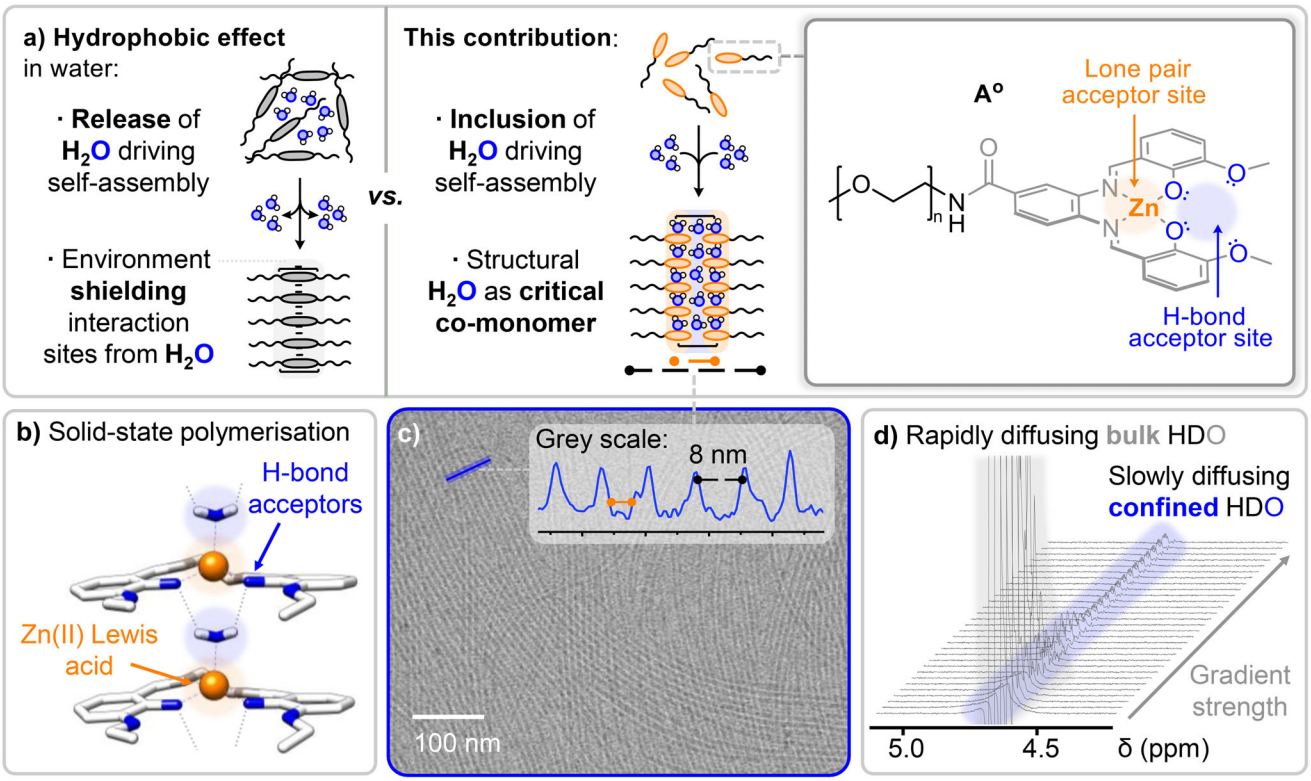

FIGURE 1 | (a) Self-assembly in water driven by the hydrophobic effect versus **A°** assembling into supramolecular fibres by inclusion of structural water. (b) Single-crystal X-ray diffraction structure of zinc(II) complex assembling into a solid-state polymer via water inclusion [44]. (c) Cryo-TEM image of 1 mM aqueous solution of **A°** with inlay of grey value profile plot. (d) Stacked HR-MAS DOSY (400 MHz, D_2O, 25°C) spectrum of **A°** (30 mM) measured at a diffusion time of 0.5 s.

of achieving assembly in water employing water as a critical comonomer, which might even determine the architecture of supramolecular polymerization, has not been realized.

There are isolated examples of water acting as a comonomer in synthetic assemblies under non-aqueous water-poor conditions [26–33]. In solvent-free systems or nonpolar organic solvents where interactions between water and the surrounding medium are unfavorable, trace water associates with the enthalpically more favorable polar sites of monomers to stabilize supramolecular polymers. In contrast, nature exploits structural water to build assemblies in aqueous environments—a feature that remains highly challenging to replicate synthetically. In supramolecular polymers formed in water, the surrounding solvent is present in large excess and strongly stabilized by its own hydrogen-bonding network. As a result, incorporation of water molecules into the assembly is generally both entropically disfavored (underlying the hydrophobic effect) and enthalpically costly. Nevertheless, translating the structural water concept to synthetic chemistry could open doors in responsive and sustainable water-borne materials. After all, water is an abundant and sustainable building block that remains remarkably underutilized as a functional and structural element in materials design.

One promising source of inspiration comes from synthetic crystalline assemblies in the solid-state and metal-organic frameworks [34–39]. Here, water plays a crucial role in regularly binding to and bridging molecules of the crystal lattice via hydrogen bonding or metal-ligand coordination. These crystalline architectures suggest that water's directionality and ability to act as both donor and acceptor can be strategically harnessed to stabilize polymeric frameworks—if appropriately confined. Translating this idea to amorphous supramolecular polymers thus would represent a new design principle for water-borne soft materials.

2 | Results and Discussion

To achieve supramolecular copolymerization of water, we turned to the self-assembly of metal complexes. These effectively confine the 3D-growth of metal-organic frameworks into two dimensions and prevent crystallization during assembly through the presence of flexible solubilizing chains [40–42]. The monomer **A°** (see Figure 1a) is a water-soluble bisphenoxyimine zinc(II) Salphen complex featuring aryl ortho-methoxy substituents and a poly(ethylene glycol) chain (PEG, M_n = 500 g/mol) [43]. **A°** was synthesized via $Zn(OAc)_2$-templated condensation of a methoxy-substituted salicylaldehyde and diamino-benzoic acid to afford the carboxylic acid intermediate, which was subsequently coupled to amino-terminated PEG via carbodiimide chemistry (see Section S02). The Zn(II) Salphen unit in **A°** features two orthogonal binding environments: a Lewis-acidic axial coordination site to the N,N,O,O Salphen ligand plane, and a hydrogen-bonding pocket defined by the two phenolate and two methoxy oxygen atoms. This dual binding motif provides both an electron-deficient site for lone-pair coordination and an electron-rich surface for hydrogen bonding—making it an ideal host for

structural water. In fact, the solid-state structure of a related Zn(II) complex (Figure 1b) comprising an ethylene backbone and lacking solubilizing chains has been reported to show polymerization in the solid-state with water as a comonomer (Zn-O distance 2.0 Å; Zn-Zn distance 5.0 Å) after crystallization from undried methanol [44]. Dissolution of $\mathbf{A^o}$ in water at 1 mM yields a clear solution that gradually increases in viscosity. Cryogenic transmission electron microscopy (cryo-TEM) reveals a dense network of spontaneously forming micrometer-long fibers with a uniform morphology, consisting of a high-contrast region of ~3–4 nm and an overall diameter of ~8 nm (Figure 1c and Section S3). Notably, no difference in fiber dimensions or morphology was observed irrespective of prior sonication or heating. Complementary, small-angle X-ray scattering (SAXS) at 50 mM indicates long, cylindrical assemblies with an estimated diameter of ~4.4 nm and lengths in the μm scale (see Section S04). Atomic force microscopy (AFM) of spin-coated dilute samples (0.05 mM) confirms the presence of thin, homogeneous fibers with heights of up to 4 nm in the dry state (see Section S05). Combined, all techniques conclusively point toward very similar dimensions of the assemblies.

Dynamic light scattering (DLS) across a dilution series reveals a remarkably low critical aggregation concentration (CAC) of 18 nM (0.018 mg/L)—lower than that of common aggregates formed through the hydrophobic effect (see Figure S76) [45, 46].

To probe the confinement of water in the assembly, we conducted diffusion-ordered ^{1}H NMR spectroscopy (DOSY) in deuterated water [47]. Here, two exponentials were needed to describe the diffusion curve associated with the HDO resonance, one corresponding to free HDO as part of the solvent phase and the other corresponding to a small, slow-diffusing fraction with a diffusion coefficient at least 40-fold reduced relative to bulk HDO. This confirms the tight association of water with the supramolecular framework (see Figure 1d).

Above a threshold concentration of 1 mM, $\mathbf{A}^\circ$ forms self-supporting hydrogels upon heating (Figure 2a and Figure S73). Variable-temperature rheology reveals a sharp sol–gel transition between 50°C and 75°C, with the storage modulus (G′) increasing from ~1 to ~400 Pa. Notably, the gel retains most of its mechanical properties upon cooling, indicating thermal hysteresis and crosslinking. Note that this is the reverse of what is often observed for gels formed by supramolecular polymerization, which disassemble upon heating. We attribute the thermally induced gelation to a decrease in the solubility of the PEG chains at elevated temperatures, promoting lateral association and entanglement of the fibres. Accordingly, further heating to the boiling point of water leads to increased phase separation of $\mathbf{A^o}$ reminiscent of a lower critical solution temperature behavior. We believe that this crosslinking process protects the fibers from supramolecular depolymerization upon heating to some extent, ensuring that the supramolecular material remains intact. Alternating shear strain measurements at variable temperatures confirm a mechanical response consistent with physical crosslinking (see Figure S82). The two counteractive trends of thermoresponsive gelation and depolymerization were investigated by performing a heating sequence (20–80°C) followed by two high shear strain cycles at 80°C to destroy the internal integrity of the gel. Subsequent cooling to 20°C revealed a sudden increase in *G'* at around 44°C, which might correspond to the onset temperature of the supramolecular polymerization (Figure 2b) of the fraction of monomers that depolymerized during heating [48, 49]. As a consequence, these rheological experiments suggest a thermally bisignate assembly as the hydrogel of $\mathbf{A^o}$ was found to gain in strength both upon heating and cooling [50].

Given that gelation results from the formation and entanglement of supramolecular fibers, rheology provides a direct means to probe structure–property relationships. First, the length of the solubilizing chain is crucial, as increasing the PEG length (from M_n = 500 to 750–5000 g/mol) leads to weaker gels upon thermal treatment, due to the formation of fewer, shorter, and less regular fibers as revealed by cryo-TEM, AFM, and rheology (see Figures S69, S75 and S83, respectively). Thus, the amphiphilicity of $\mathbf{A}^\circ$, combining water-soluble PEG with the more hydrophobic Salphen unit, plays a key role in providing a platform for water confinement, with increased overall hydrophilicity disrupting supramolecular polymerization.

To test the importance of the hydrogen-bond acceptor pocket in $\mathbf{A^o}$, we examined structural analogues $\mathbf{A^m}$ and $\mathbf{A^p}$, which bear methoxy groups in the *meta*- and *para*-positions, respectively. Neither $\mathbf{A^m}$ nor $\mathbf{A^p}$ forms a hydrogel as demonstrated by rheology (Figure 2c). Accordingly, a very limited ability to form fibers is observed (cryo-TEM; see Figures S70 and S71). This shows that the specific arrangement of the four oxygen atoms in $\mathbf{A^o}$ is critical for effective assembly in water. Disruption of this binding geometry prevents structural water confinement required for self-assembly.

Subsequently, we probed the role of axial coordination by the zinc(II) center. Addition of Lewis bases such as triethylamine or pyridine to $\mathbf{A^o}$ inhibits gelation (see Figure S84). These bases are known to coordinate axially to Zn(II), blocking water coordination, thus suppressing the water-mediated assembly pathway [41, 51]. Similarly, the nickel(II) analogue of $\mathbf{A^o}$, which is significantly less Lewis acidic and chemically softer according to Pearsons' HSAB concept, fails to coordinate the hard oxygen lone-pairs of water effectively and does not form hydrogels [41]. Exploiting this sensitivity, we could demonstrate that in situ transmetallation on the rheometer stage can actively disassemble the hydrogel. Treatment of a hydrogel formed from $\mathbf{A^o}$ with $Ni(OAc)_2$ followed by a second heating-cooling sequence achieves exchange of the zinc for nickel—as further confirmed by NMR spectroscopy—and induces a gel–sol transition (Figure 2d and Figure S86). Similar behavior was observed for transmetallation with Cu(II) and Co(II) (see Figure S87). This underpins the potential of these materials to act as chemosensors for metal salts and Lewis bases by controlling the incorporation of structural water, which affects macroscopic properties.

Next, we aimed to mechanistically decouple water-mediated assembly from classical stacking as commonly observed for Zn(II) Salphen and other metal-containing derived monomers [52–57]. Therefore, we synthesized the hydrophobic analogues $\mathbf{B^o}$, $\mathbf{B^m}$, and $\mathbf{B^p}$, replacing the PEG chain with two aliphatic tails (Figure 3a), leading to solubility in organic solvents. Interestingly, $\mathbf{B^p}$ forms organogels in mesitylene or toluene while $\mathbf{B^o}$ and $\mathbf{B^m}$ do not. In $\mathbf{B^p}$ the solubilizing chains do not exhibit any thermal responsiveness so that disassembly occurs upon heating together with liquification of the gel (Figure 3b). Transmission

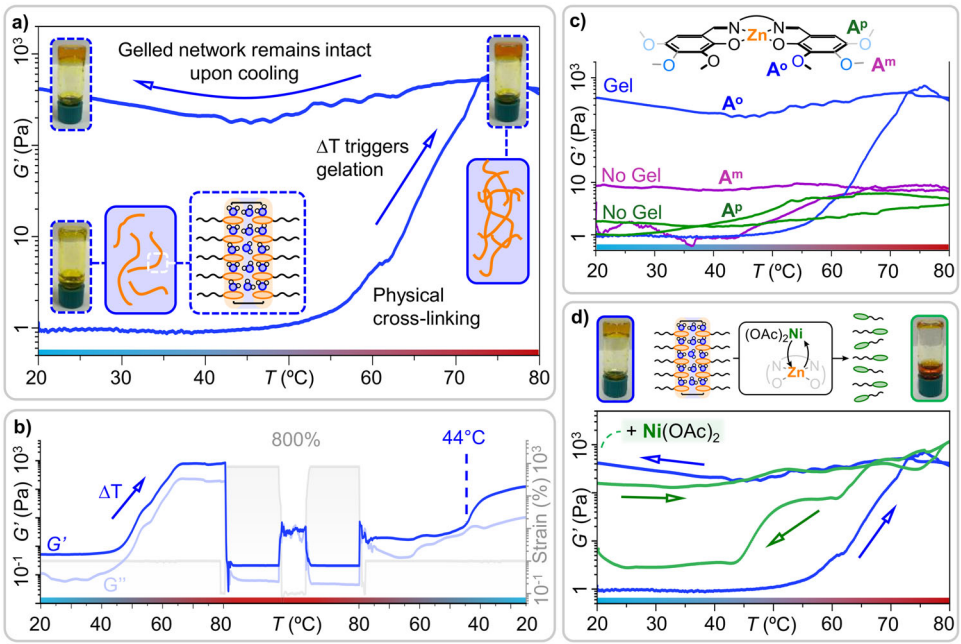

FIGURE 2 | (a) Variable-temperature rheology of $\mathbf{A^o}$ revealing thermoresponsive sol-gel transition due to entanglement of fibers. (b) Three-step rheology sequence consisting of a heating sequence, followed by two high-strain cycles and a subsequent cooling sequence. (c) Dependence of rheology on substituent pattern. (d) Transmetallation of $\mathbf{A^o}$ with $Ni(OAc)_2$ inducing gel-sol transition.

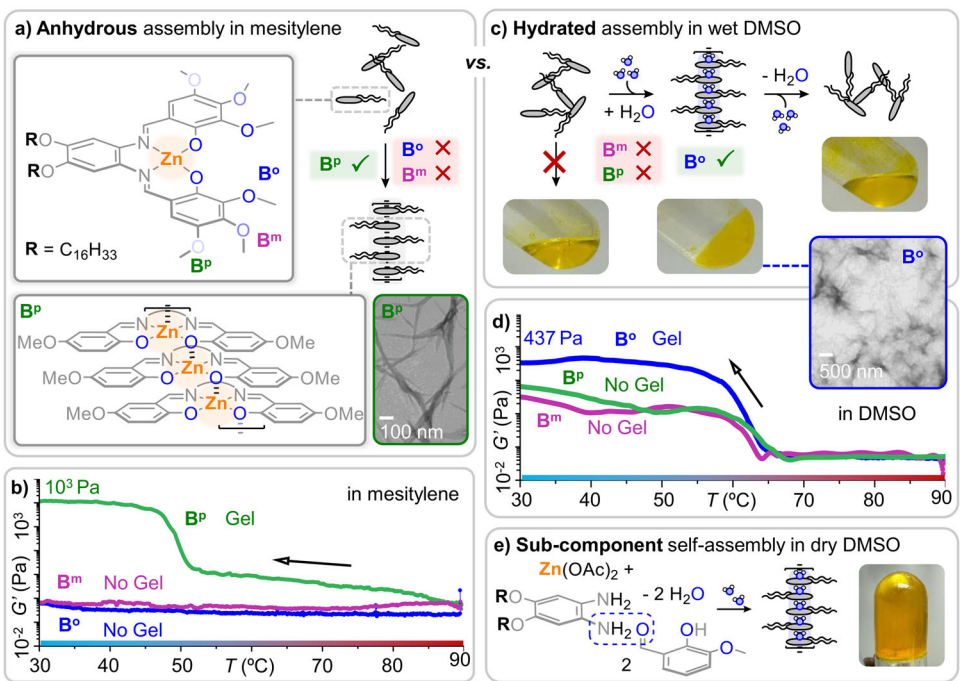

FIGURE 3 | (a) Anhydrous self-assembly of $\mathbf{B^p}$ in non-coordinating aromatic solvents via formation of stacks without water inclusion; TEM image of $\mathbf{B^p}$ obtained upon evaporation of a THF solution shown. (b) Variable-temperature rheology of 3 mM solutions of $\mathbf{B^o}$, $\mathbf{B^m}$, and $\mathbf{B^p}$ in mesitylene. (c) Hydrated self-assembly of $\mathbf{B^o}$ in DMSO depending on the addition of water, with optical photographs of a 5 mM solution before and after the addition of (0.1 v%) water and after removal of the water content under reduced pressure and 50°C; TEM image of $\mathbf{B^o}$ obtained upon evaporation of wet DMSO solution. (d) Variable temperature rheology of 3 mM solutions of $\mathbf{B^o}$, $\mathbf{B^m}$, and $\mathbf{B^p}$ in wet DMSO. (e) Sub-component self-assembly of $\mathbf{B^o}$ (10 mM) from building blocks of $\mathbf{B^o}$ in dry DMSO.

electron microscopy (TEM) of $\mathbf{B}^{p}$ reveals the formation of fibrous aggregates approx. 50–100 nm in thickness (see Figure S90). Notably, the presence of a single amide-coupled N-alkyl chain—as opposed to two ether-bonded chains as in $\mathbf{B}^{p}$—leads to similar thermal profiles of the organogel and a reduced overall gel strength (see Figure S85). Such aggregates of zinc(II) Salphens in organic solutions have been shown to form through direct stacking of complexes via interaction of the zinc(II) center of one complex with the phenolate oxygen of another complex. This assembly mode occurs without water intercalation and is not accessible to $\mathbf{B}^{o}$ due to *ortho*/*meta*-methoxy sterics, which cannot form organogels. The situation is reversed in wet DMSO (see Figure 3c,d), a solvent miscible with water. Note that DMSO is a coordinating solvent which typically blocks the self-assembly of Zn(II) Salphens due to axial coordination of the solvent to the Zn(II) center, suppressing stacking. Nevertheless, solutions of $\mathbf{B}^{\circ}$ form stiff organogels at 3 mM, while $\mathbf{B}^{m}$ and $\mathbf{B}^{p}$ do not. Importantly, the gelation of $\mathbf{B}^{o}$ critically depends on the water content in DMSO, and thermogravimetric analysis supports water binding to $\mathbf{B}^{o}$ (see Figure S111) aligned with our structural model (see below). In dried DMSO, self-assembly and gelation are not observed, but the addition of minimal water (0.1 v%) followed by thermal equilibration through heating and slow cooling to room temperature results in gelation. TEM analysis reveals the formation of clustered thin fibers (see Figure S91). Removing the added water at 50°C and reduced pressure reverses the process, and no gelation occurs upon cooling to room temperature. Combined, this confirms that the *ortho* methoxy substituted assembly units in $\mathbf{B}^{o}$—like $\mathbf{A}^{o}$—require structural water for supramolecular polymerization, establishing a mechanistic orthogonality to classical direct stacking without water participation.

The synthesis of $\mathbf{B}^{o}$ from the diamine, the aldehyde, and the $Zn(OAc)_2$ is an imine condensation reaction during which water is released. Supramolecular copolymerization of water occurs so efficiently that the water molecules released during condensation can be harnessed to obtain metal-organic fibres directly from the sub-components of $\mathbf{B}^{o}$ (see Figure 3e). Accordingly, heating a solution of aldehyde, imine, and zinc source to 80°C in dry DMSO, followed by cooling to room temperature, leads to gelation of the mixture. NMR spectroscopy confirms the selective formation of $\mathbf{B}^{o}$ (see Figure S81).

To rationalize the structural basis of water-mediated assembly, we turned to density functional theory (DFT) (see Section S12). We first modelled supramolecular polymerization in the absence of water, constructing dimers to pentamers of Zn(II) Salphen cores without solubilizing chains ($\mathbf{A'}^{o}$, $\mathbf{A'}^{m}$, $\mathbf{A'}^{p}$). For computational efficiency, the DFT models use complexes without solubilizing chains in the gas phase; therefore, the conclusions should be interpreted with caution within the context of these minimal models. Upon optimization, all systems could form stable dimers featuring Zn_2O_2 coordination cores—a common motif in this class of complexes [43]. However, only $\mathbf{A'}^{p}$ maintained trimeric, tetrameric, and pentameric structures; $\mathbf{A'}^{o}$ and $\mathbf{A'}^{m}$ dissociated beyond the dimer state, likely due to steric clashes from the *ortho*- and *meta*-methoxy substituents. These results are consistent with experimental results, where only $\mathbf{B}^{p}$ assembles in nonpolar solvents via classical stacking. These calculations were designed to isolate intrinsic coordination and hydrogen-bonding preferences, rather than to reproduce the complete solvated assemblies.

In stark contrast, when explicit water molecules were introduced to bridge the Zn(II) centers, $\mathbf{A'}^{\circ}$ formed stable water-mediated stacks up to the pentamer level while $\mathbf{A'}^{m}$ and $\mathbf{A'}^{p}$ collapse during optimization, forming irregular structures (Figure 4a). The ability of $\mathbf{A'}^{o}$ to copolymerize with water arises from the spatial co-localization of the hydrogen-bond acceptor sites: both the phenolate and ortho-methoxy oxygens reside on the same face of the molecule, forming a convergent hydrogen bond acceptor pocket. Atomic charge distribution maps confirm localized negative potential in this region (see Figure S99). In contrast, $\mathbf{A'}^{m}$ and $\mathbf{A'}^{p}$ display divergent hydrogen-bonding vectors, where interactions with the methoxy and phenolate groups oppose each other. Hence, the presence of intercalated water transforms $\mathbf{A'}^{o}$ into a cooperative, energetically favored assembly unit. Moreover, dimers of $\mathbf{A'}^{o}$ can accommodate not only single bridging water but also larger hydrogen-bonded clusters, which are energetically stable (Figure 4b). We then included the amide unit—linking the PEG chains to the Salphen core in $\mathbf{A}^{o}$—as well as one representative ethylene glycol unit ($\mathbf{A''}^{o}$) in our DFT model. Studying dimers of $\mathbf{A''}^{o}$ with intercalated water, it becomes evident that additional water molecules bridge between the amide functionalities of the assemblies, thereby precluding direct hydrogen bonding between these as the dominant interaction behind self-assembly.

To probe this, we conducted hydrogen/deuterium exchange mass spectrometry (HDX-MS; Section S13) [58]. Diluting a solution of preassembled $\mathbf{A}^{o}$ in water (3 mM) with a 100-fold excess of D_2O, followed by immediate ESI-MS measurement, reveals complete exchange of all amide protons for deuterium. This confirms that the amide groups are accessible to the surrounding medium, making it unlikely that they participate in persistent hydrogen bonding or are buried in hydrophobic regions, as such environments typically lead to slow exchange rates [59].

Closer inspection of cryo-TEM images at lower concentrations (0.04 mM) reveals a more resolved morphology: the fibers appear "hollow", suggesting a tubular arrangement with a water-filled inner channel (Figure 4c). 3D reconstruction using single-particle analysis (SPA), a method commonly applied for biological specimens but rarely for synthetic polymers, provided deeper insights into the tubular architecture of $\mathbf{A}^{o}$ [60, 61]. Reference-free 2D classification of ~1.1 million fiber segments extracted from ~1400 micrographs reveals lateral association of individual strands of high density, likely arising from the electron-rich Zn(II) Salphen units (Figure 4d). The most prominent class averages show two walls of high density (~10 Å each) flanking a central low-density region (~8 Å). Furthermore, Fourier transform analysis of the fiber segments reveals a diffuse water ring spaced at ~3.6–3.7 Å—consistent with confined water—as well as multiple defined spots around 4 Å and a single layer line at ~4.8 Å indicative of a repetitive unit [62]. X-ray diffraction measurements of hydrogels at 50 mM support this morphology in bulk samples, showing reflections corresponding to periodicities at similar distances (see Section S14).

The density map—obtained by helical reconstruction with a global resolution of 2.3 Å—revealed a tubular arrangement of eight separate strands, which could be back-projected into 2D class averages with excellent agreement (see Section S15). The repetitive pattern allowed us to tentatively fit individual

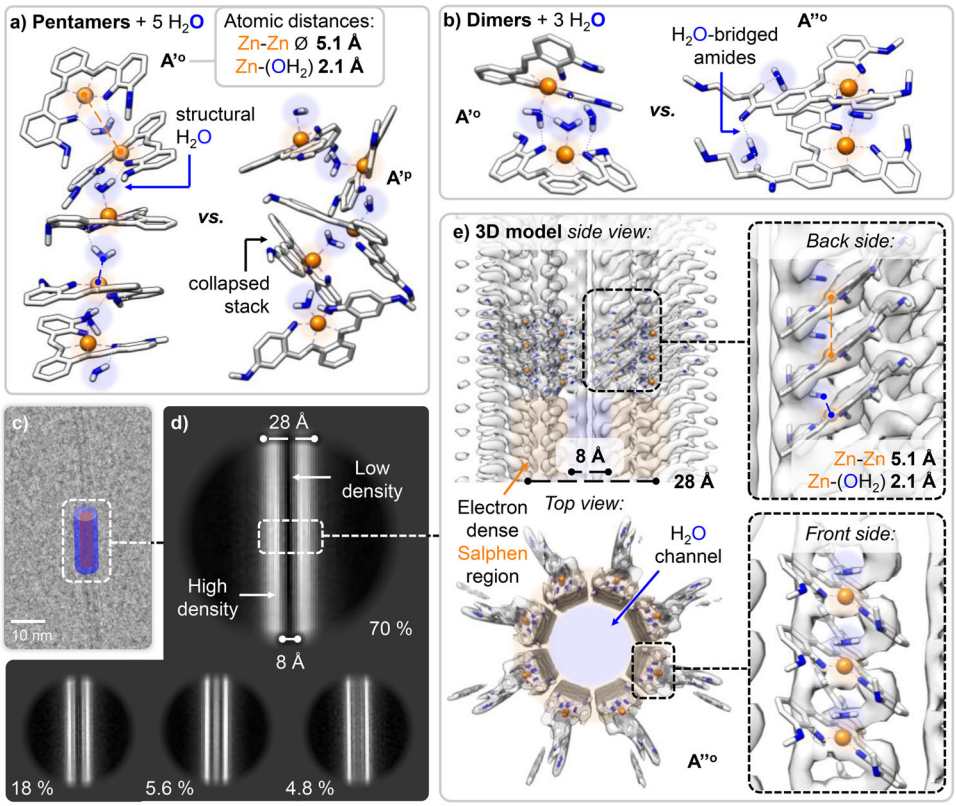

FIGURE 4 | DFT optimized structures of (a) pentamers of stacked $\mathbf{A'^{o}}$ with structural water molecules versus the collapsed stack of $\mathbf{A'^{p}}$, respectively, and (b) dimers of $\mathbf{A'^{o}}$ versus $\mathbf{A''^{o}}$ (including amide groups) with three intercalated water molecules. (c) Cryo-TEM image of $\mathbf{A^{o}}$ showing a hollow fiber. (d) Selected class averages after reference-free 2D classification of fiber segments using single particle analysis (SPA). (e) 3D model of the tubular fibers obtained by fitting of 24 copies of $\mathbf{A''^{o}}$ (including amide groups) to the cryo-EM density map after reconstruction (decreased contour level in "front side" inlay).

molecules of $\mathbf{A'''^{o}}$ into the map and thereby propose a structural model on the molecular level (Figure 4e). Notably, the stacking geometries obtained from independent DFT-optimized minimal models placed into the cryo-EM density with high fidelity; alternative plausible arrangements failed to fit. Accordingly, $\mathbf{A^{o}}$ assembles into regular stacks of monomers tilted by ~42° to the tubular axis. The inter-molecular distances are in striking agreement with our DFT results for pentamers of $\mathbf{A'^{o}}$ with Zn-Zn distances of 5.1 Å and tightly coordinated structural water molecules in between each monomer unit. In this tubular arrangement of eight Zn(II) Salphen-water stacks, the *ortho*-methoxy groups that can accept hydrogen bonds face inward, thereby creating a hydrophilic environment within the tube interior. The amide groups on the tube exterior are further aligned on top of each other without direct interaction, likely bridged by water molecules as suggested by the HDX-MS experiments. The increasing loss of density for the extended PEG chains attached to the amides reflects their high flexibility, which prevents them from being resolved by SPA. Nevertheless, the tubular arrangement of chromophores promises applications in optoelectronics and transport.

Based on the observation that the external amide functionalities of $\mathbf{A^{o}}$ are not trapped in direct interactions, we explored whether these orthogonal interaction sites could mediate recognition and sensing of biologically relevant small molecules. Strikingly, addition of L-alanine (0.1 M) to aqueous solutions of $\mathbf{A^{o}}$ induces a pronounced circular dichroism (CD) signal in the chromophore region (250–500 nm), reflecting chiral information transfer from the surrounding medium to the supramolecular stack (Figure 5a) [63]. No signal is observed with L-phenylalanine or L-leucine under identical conditions, suggesting that fibers of $\mathbf{A^{o}}$ can chemoselectively discriminate between biomolecules via chiral induction. Importantly, in the disassembled state in the presence of a Lewis base, no transfer of chiral information from L-alanine to $\mathbf{A^{o}}$ is observed. Cryo-TEM reveals the appearance of small aggregate fragments upon alanine addition, which are mostly associated to the regular fibers (Figure 4b). These additional structures also cause a change in the size-distribution pattern in multiangle light scattering measurements (MALS) and coincide with a reduced critical gelation concentration (see Figures S77 and S104, respectively)—highlighting the emergence of the alternate barbed wire morphology. Importantly, the same CD signal appears whether L-alanine is added before or after assembly of fibers from $\mathbf{A^{o}}$, indicating that chiral information is transferred via surface binding (see Figure S105).

To investigate this hypothesis, we extended our DFT model by introducing L-alanine molecules in their zwitterionic form—as present in neutral aqueous solution—into a pentamer of $\mathbf{A'''^{o}}$. In the initial configuration, the L-alanine molecules were positioned adjacent to the amide functionalities, as this was considered the most plausible site for chirality transfer (see Figure S100). Whereas the pentameric stack without L-alanine

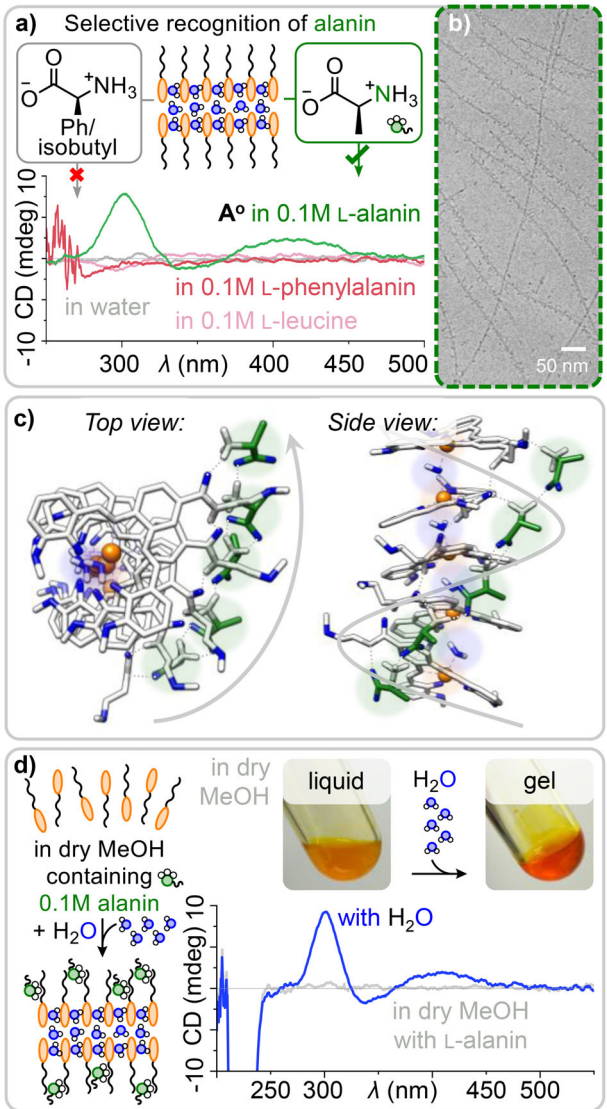

FIGURE 5 | (a) Recognition of L-alanin over L-phenylalanin and L-leucine by **A°** fibers transferring chiral information as seen by CDspectroscopy. (b) Cryo-TEM image of **A°** in 0.1 M L -alanin solution, revealing a barbed wire type morphology. (c) DFT optimized structure of pentamer of **A″°** and L-alanine (green, zwitterionic form) showing induction of supramolecular chirality. (d) Water addition to **A°** in dry methanolic 0.1 M L-alanin solution triggers self-assembly (inlay image of gelation) and transfer of chiral information.

exhibits no helicity (Figure 4a), the presence of L-alanine led to bridging interactions with the amide bonds of **A′′°**, thereby transferring chiral information and inducing a helical rotation within the pentameric stack (Figure 5c). Although this model does not account for the tubular superstructure or solvent effects, it highlights the potential for chirality induction at the molecular level, which could translate onto the supramolecular geometry and ultimately drive the observed morphological changes.

To probe the molecular origin of the amino acid specific recognition, we investigated L-lactate, a structural analogue of L-alanine with an OH in place of an NH_3^+ group but observed no transfer of chiral information (see Figure S106). Moreover, elevating the pH from 7 to 10 (zwitterion → anion) attenuates the CD signal, implicating hydrogen bonding between the protonated amine and the exterior amide groups of **A°** fibres as the key interaction (see Figure S107). Hence, the selectivity for L-alanine over L-phenylalanine and L-leucine likely results from a steric mismatch with the geometry of the amino-acid with the fibre exterior.

Finally, we demonstrate that this chiral communication depends critically on structural water. In dry ethanol, where **A°** does not assemble, L-alanine induces no CD signal. However, the addition of just 0.1 vol% water triggers self-assembly, gelation, and a chiral response (Figure 5d). Thus, structural water not only enables assembly but also molecular-to-supramolecular chiral transduction.

3 | Conclusion

In summary, we introduce a soft metal–organic supramolecular material in which structural water functions as an active design element, enabling the formation of adaptive, chiral, and dynamically reconfigurable fiber gels. Through precise molecular design combining Lewis-acidic zinc(II) centers and convergent hydrogen-bond acceptor pockets, water is no longer a passive medium but acts as a structural co-monomer that drives hierarchical self-assembly in bulk aqueous environments. Single-particle analysis reveals tubular metal–organic fibers stabilized by confined water molecules, which translate molecular features into macroscopic material behavior. These hydrated fibers form thermoresponsive hydrogels with bisignate mechanical transitions and mediate chiral recognition through water-assisted information transfer. Together, these findings establish structural water as a versatile and sustainable design element for next-generation supramolecular materials, bridging molecular coordination chemistry with adaptive and reconfigurable material functionality.

Acknowledgements

We thank the "Deutsche Forschungsgemeinschaft 492723217" (CRC 1585 Multitrans, CRC 1449 Dynamic Hydrogels at Biointerfaces, Core Facility BioSupraMol, INST 130/1064-1 FUGG to Freie Universität Berlin) and the "European Research Council" (ERC Advanced Grant SupraVir, 101055416). The authors thank the experimental team of the proposal I-20240767, Richard Neubert, Anika C. Lehmann and Maxim Kaulfers, and the local contact Silvio Haas for their assistance during the SAXS test measurement. Furthermore, Josef Breu is acknowledged for providing access to the XRD instrument.

Open access funding enabled and organized by Projekt DEAL.

Conflicts of Interest

The authors declare no conflicts of interest.

Data Availability Statement

The data that support the findings of this study are available in the supplementary material of this article.

References

1. A. Albers, S. Kuberasivakumaran, Z. Fernández, et al., "Size-Controlled Self-Assembly for Bimodal In Vivo Imaging," *Angewandte Chemie*

International Edition 64 (2025): 202500144, https://doi.org/10.1002/anie.202500144.

2. F. Esteve, Z. Yang, and J.-M. Lehn, "Emerging Complex Behavior Driven by Self-Organization: Dynamic Covalent Libraries of Acylhydrazones in Water," *Journal of the American Chemical Society* 147 (2025): 28408–28418, https://doi.org/10.1021/jacs.5c09521.

3. S. D. P. Fielden, "Kinetically Controlled and Nonequilibrium Assembly of Block Copolymers in Solution," *Journal of the American Chemical Society* 146 (2024): 18781–18796, https://doi.org/10.1021/jacs.4c03314.

4. E. G. Percástegui, J. Mosquera, T. K. Ronson, A. J. Plajer, M. Kieffer, and J. R. Nitschke, "Waterproof Architectures Through Subcomponent Self-assembly," *Chemical Science* 10 (2019): 2006–2018, https://doi.org/10.1039/C8SC05085F.

5. W. Han, W. Xiang, Q. Li, et al., "Water Compatible Supramolecular Polymers: Recent Progress," *Chemical Society Reviews* 50 (2021): 10025–10043, https://doi.org/10.1039/D1CS00187F.

6. N. S. Nagornova, T. R. Rizzo, and O. V. Boyarkin, "Interplay of Intra- and Intermolecular H-Bonding in a Progressively Solvated Macrocyclic Peptide," *Science* 336 (2012): 320–323, https://doi.org/10.1126/science.1218709.

7. Y. Umena, K. Kawakami, J.-R. Shen, and N. Kamiya, "Crystal Structure of Oxygen-Evolving Photosystem II at a Resolution of 1.9 Å," *Nature* 473 (2011): 55–60, https://doi.org/10.1038/nature09913.

8. S. Holvec, C. Barchet, A. Lechner, et al., "The Structure of the Human 80S Ribosome at 1.9 Å Resolution Reveals the Molecular Role of Chemical Modifications and Ions in RNA," *Nature Structural & Molecular Biology* 31 (2024): 1251–1264, https://doi.org/10.1038/s41594-024-01274-x.

9. J. Bella, B. Brodsky, and H. M. Berman, "Hydration Structure of a Collagen Peptide," *Structure (London, England)* 3 (1995): 893–906, https://doi.org/10.1016/S0969-2126(01)00224-6.

10. H. Fu, J. Huang, J. J. B. van der Tol, et al., "Supramolecular Polymers form Tactoids Through Liquid–Liquid Phase Separation," *Nature* 626 (2024): 1011–1018, https://doi.org/10.1038/s41586-024-07034-7.

11. L. Ye, X. Dong, C. Wang et al., "Helical Protein Nanotubules Assembled From Sacrificial Supramolecular Polymers," *Nature Synthesis* 4 (2025): 562–572, https://doi.org/10.1038/s44160-024-00726-y.

12. K. Liu, A. Blokhuis, C. van Ewijk, et al., "Light-driven Eco-evolutionary Dynamics in a Synthetic Replicator System," *Nature Chemistry* 16 (2024): 79–88, https://doi.org/10.1038/s41557-023-01301-2.

13. J. Boekhoven, W. E. Hendriksen, G. J. M. Koper, R. Eelkema, and J. H. van Esch, "Transient Assembly of Active Materials Fueled by a Chemical Reaction," *Science* 349 (2015): 1075–1079, https://doi.org/10.1126/science.aac6103.

14. S. Bianco, M. Hasan, A. Ahmad, et al., "Mechanical Release of Homogenous Proteins From Supramolecular Gels," *Nature* 631 (2024): 544–548, https://doi.org/10.1038/s41586-024-07580-0.

15. S. Chen, R. Costil, F. K.-C. Leung, and B. L. Feringa, "Self-Assembly of Photoresponsive Molecular Amphiphiles in Aqueous Media," *Angewandte Chemie International Edition* 60 (2021): 11604–11627, https://doi.org/10.1002/anie.202007693.

16. L. Borsdorf, L. Herkert, N. Bäumer, et al., "Pathway-Controlled Aqueous Supramolecular Polymerization via Solvent-Dependent Chain Conformation Effects," *Journal of the American Chemical Society* 145 (2023): 8882–8895, https://doi.org/10.1021/jacs.2c12442.

17. P. Khanra, P. Rajdev, and A. Das, "Seed-Induced Living Two-Dimensional (2D) Supramolecular Polymerization in Water: Implications on Protein Adsorption and Enzyme Inhibition," *Angewandte Chemie International Edition* 136 (2024): 202400486.

18. N. Fukaya, S. Ogi, H. Sotome, et al., "Impact of Hydrophobic/Hydrophilic Balance on Aggregation Pathways, Morphologies, and Excited-State Dynamics of Amphiphilic Diketopyrrolopyrrole Dyes in Aqueous Media," *Journal of the American Chemical Society* 144 (2022): 22479–22492, https://doi.org/10.1021/jacs.2c07299.

19. L. Su, J. Mosquera, M. F. J. Mabesoone, et al., "Dilution-induced Gel-sol-gel-sol Transitions by Competitive Supramolecular Pathways in Water," *Science* 377 (2022): 213–218, https://doi.org/10.1126/science.abn3438.

20. H. Duijs, M. Kumar, S. Dhiman, and L. Su, "Harnessing Competitive Interactions to Regulate Supramolecular "Micelle-Droplet-Fiber" Transition and Reversibility in Water," *Journal of the American Chemical Society* 146 (2024): 29759–29766, https://doi.org/10.1021/jacs.4c11285.

21. F. V. de Graaf, C. Zoister, B. Schade, et al., "Amplification of Asymmetry via Structural Transitions in Supramolecular Polymer–Surfactant Coassemblies," *Journal of the American Chemical Society* 147 (2025): 17468–17476.

22. F. Xu, S. Crespi, G. Pacella, et al., "Dynamic Control of a Multistate Chiral Supramolecular Polymer in Water," *Journal of the American Chemical Society* 144 (2022): 6019–6027, https://doi.org/10.1021/jacs.2c01063.

23. B. Trappmann, K. Ludwig, M. R. Radowski, et al., "A New Family of Nonionic Dendritic Amphiphiles Displaying Unexpected Packing Parameters in Micellar Assemblies," *Journal of the American Chemical Society* 132 (2010): 11119–11124, https://doi.org/10.1021/ja101523v.

24. J. H. Ortony, B. Qiao, C. J. Newcomb, et al., "Water Dynamics From the Surface to the Interior of a Supramolecular Nanostructure," *Journal of the American Chemical Society* 139 (2017): 8915–8921.

25. T. Ivanov, T. P. Doan-Nguyen, M. A. Belahouane, et al., *Macromolecular Rapid Communications* 45 (2024): 2400626.

26. N. J. Van Zee, B. Adelizzi, M. F. J. Mabesoone, et al., "Potential Enthalpic Energy of Water in Oils Exploited to Control Supramolecular Structure," *Nature* 558 (2018): 100–103, https://doi.org/10.1038/s41586-018-0169-0.

27. S. Dong, J. Leng, Y. Feng, et al., "Structural Water as an Essential Comonomer in Supramolecular Polymerization," *Science Advances* 3 (2017): aao0900, https://doi.org/10.1126/sciadv.aao0900.

28. H. Arazoe, D. Miyajima, K. Akaike, et al., "An Autonomous Actuator Driven by Fluctuations in Ambient Humidity," *Nature Materials* 15 (2016): 1084–1089, https://doi.org/10.1038/nmat4693.

29. N. J. Van Zee, M. F. J. Mabesoone, B. Adelizzi, A. R. A. Palmans, and E. W. Meijer, "Biasing the Screw-Sense of Supramolecular Coassemblies Featuring Multiple Helical States," *Journal of the American Chemical Society* 142 (2020): 20191–20200, https://doi.org/10.1021/jacs.0c10456.

30. Q. Zhang, T. Li, A. Duan, S. Dong, W. Zhao, and P. J. Stang, "Formation of a Supramolecular Polymeric Adhesive via Water–Participant Hydrogen Bond Formation," *Journal of the American Chemical Society* 141 (2019): 8058–8063.

31. X. Li, J. Lai, Y. Deng, J. Song, G. Zhao, and S. Dong, "Supramolecular Adhesion at Extremely Low Temperatures: A Combined Experimental and Theoretical Investigation," *Journal of the American Chemical Society* 142 (2020): 21522–21529, https://doi.org/10.1021/jacs.0c10786.

32. Q. Xu, P. Szymoniak, M. A. Kolmangadi, et al., "Molecular Engineering of Supramolecular Polymer Adhesive With Confined Water and a Single Crown Ether," *Chemical Science* 16 (2025): 1995–2003, https://doi.org/10.1039/D4SC06771A.

33. Y. Zhang, S. Zhang, H. Wu, et al., "Evolution of Transient Luminescent Assemblies Regulated by Trace Water in Organic Solvents," *Journal of the American Chemical Society* 144 (2022): 19410–19416, https://doi.org/10.1021/jacs.2c07349.

34. P. Xing, Y. Li, Y. Wang, et al., "Water-Binding-Mediated Gelation/Crystallization and Thermosensitive Superchirality," *Angewandte Chemie International Edition* 57 (2018): 7774–7779, https://doi.org/10.1002/anie.201802825.

35. H. J. Cho, D. Y. Jeong, H. Moon, et al., "Unconventional Assemblies of Bisacylhydrazones: The Role of Water for Circularly Polarized Luminescence," *Aggregate* 3 (2022): 168, https://doi.org/10.1002/agt2.168.

36. J. F. Woods, K. Zhang, J. Peterschmitt, et al., "A Supramolecular Nanosheet Assembled From Carpyridines and Water," *Journal of the*

American Chemical Society 147 (2025): 18380–18385, https://doi.org/10.1021/jacs.4c17024.

37. A. Vidyasagar and K. M. Sureshan, "Stoichiometric Sensing to Opt Between Gelation and Crystallization," *Angewandte Chemie International Edition* 54 (2015): 12078–12082, https://doi.org/10.1002/anie.201506544.

38. L. Zhang, R.-C. Gao, X. Liu, B. Zhang, L. Hou, and Y.-Y. Wang, "Unique H2O Vortex in One New MOF Material Strengthening C3H6 Adsorption and Unprecedented Purification From C2H4/C3H8/C3H6 Mixtures," *Advanced Functional Materials* 35 (2025): 2420927, https://doi.org/10.1002/adfm.202420927.

39. S. Chen, Z. Zhang, W. Chen, et al., "Understanding Water Reaction Pathways to Control the Hydrolytic Reactivity of a Zn Metal-Organic Framework," *Nature Communications* 15 (2024): 10776, https://doi.org/10.1038/s41467-024-54493-7.

40. Y.-S. Wei, Z. Fan, C. Luo, and S. Horike, "Desolvation of Metal Complexes to Construct Metal-Organic Framework Glasses," *Nature Synthesis* 3 (2024): 214–223.

41. M. R. Stühler, H. Makki, D. Silbernagl, et al., "Flexibility and Dynamicity Enhances and Controls Supramolecular Self-Assembly of Zinc(II) Metallogels," *Advanced Functional Materials* (2025): 2507793.

42. M. R. Stühler and A. J. Plajer, "Supramolecular Polymerization and Self-Assembly of Transition Metal Complexes," *Polymer Chemistry* 16 (2025): 2799–2810.

43. A. W. Kleij, "Zinc-centred Salen Complexes: Versatile and Accessible Supramolecular Building Motifs," *Dalton Transactions* (2009): 4635–4639, https://doi.org/10.1039/b902866h.

44. H. Y. Liu, C. Li, and J. J. Ma, "New Vanadium and Zinc Complexes With Schiff Base Ligand N,N′-bis(3-ethoxy-2-hydroxybenzylidene)Ethylenediamine: Synthesis, Structures, and Biochemical Properties," *Russian Journal of Coordination Chemistry* 40 (2014): 240–245, https://doi.org/10.1134/S1070328414040046.

45. C. Oerlemans, W. Bult, M. Bos, G. Storm, J. F. W. Nijsen, and W. E. Hennink, "Polymeric Micelles in Anticancer Therapy: Targeting, Imaging and Triggered Release," *Pharmaceutical Research* 27 (2010): 2569–2589, https://doi.org/10.1007/s11095-010-0233-4.

46. D. Braatz, J. H. Peter, M. Dimde, et al., "Dendritic Polyglycerolsulfate-SS-poly(ester amide) Micelles for the Systemic Delivery of Docetaxel: Pushing the Limits of Stability Through the Insertion of π–π Interactions," *Journal of Materials Chemistry B* 11 (2023): 3797–3807.

47. K. Oka, T. Shibue, N. Sugimura, Y. Watabe, B. Winther-Jensen, and H. Nishide, "Long-lived Water Clusters in Hydrophobic Solvents Investigated by Standard NMR Techniques," *Scientific Reports* 9 (2019): 223, https://doi.org/10.1038/s41598-018-36787-1.

48. M. Wehner and F. Würthner, "Supramolecular Polymerization Through Kinetic Pathway Control and Living Chain Growth," *Nature Reviews Chemistry* 4 (2020): 38–53, https://doi.org/10.1038/s41570-019-0153-8.

49. S. Datta, H. Itabashi, T. Saito, and S. Yagai, "Secondary Nucleation as a Strategy toward Hierarchically Organized Mesoscale Topologies in Supramolecular Polymerization," *Nature Chemistry* 17 (2025): 477–492, https://doi.org/10.1038/s41557-025-01764-5.

50. K. Venkata Rao, D. Miyajima, A. Nihonyanagi, and T. Aida, "Thermally Bisignate Supramolecular Polymerization," *Nature Chemistry* 9 (2017): 1133–1139, https://doi.org/10.1038/nchem.2812.

51. N. Sasaki, J. Kikkawa, Y. Ishii, et al., "Multistep, Site-selective Noncovalent Synthesis of Two-dimensional Block Supramolecular Polymers," *Nature Chemistry* 15 (2023): 922–929, https://doi.org/10.1038/s41557-023-01216-y.

52. J. K.-H. Hui, Z. Yu, and M. J. MacLachlan, "Supramolecular Assembly of Zinc Salphen Complexes: Access to Metal-Containing Gels and Nanofibers," *Angewandte Chemie, International Edition in English* 119 (2007): 8126–8129, https://doi.org/10.1002/ange.200702680.

53. K. Fu, Y. Zhao, and G. Liu, "Pathway-directed Recyclable Chirality Inversion of Coordinated Supramolecular Polymers," *Nature Communications* 15 (2024): 9571, https://doi.org/10.1038/s41467-024-53928-5.

54. A. Aliprandi, M. Mauro, and L. De Cola, "Controlling and Imaging Biomimetic Self-assembly," *Nature Chemistry* 8 (2016): 10–15, https://doi.org/10.1038/nchem.2383.

55. C. Montañez-Moyano, Y. Xue, M. V. Cappellari, et al., "Controlling Asymmetry Amplification Through Supramolecular Polymorphism," *Angewandte Chemie International Edition* (2025): 202509031.

56. G. Salassa, M. J. J. Coenen, S. J. Wezenberg, et al., "Extremely Strong Self-Assembly of a Bimetallic Salen Complex Visualized at the Single-Molecule Level," *Journal of the American Chemical Society* 134 (2012): 7186–7192, https://doi.org/10.1021/ja3030802.

57. Q. Wan, W.-P. To, X. Chang, and C.-M. Che, "Controlled Synthesis of PdII and PtII Supramolecular Copolymer with Sequential Multiblock and Amplified Phosphorescence," *Chem* 6 (2020): 945–967.

58. X. Lou, R. P. M. Lafleur, C. M. A. Leenders, et al., "Dynamic Diversity of Synthetic Supramolecular Polymers in Water as Revealed by Hydrogen/Deuterium Exchange," *Nature Communications* 8 (2017): 15420, https://doi.org/10.1038/ncomms15420.

59. X. Lou, S. M. C. Schoenmakers, J. L. J. van Dongen, et al., "Elucidating Dynamic Behavior of Synthetic Supramolecular Polymers in Water by Hydrogen/Deuterium Exchange Mass Spectrometry," *Journal of Polymer Science* 59 (2021): 1151–1161, https://doi.org/10.1002/pol.20210011.

60. H. Zhang, X. Li, J. Liu, Y.-Q. Lan, and Y. Han, "Advancing Single-Particle Analysis in Synthetic Chemical Systems: A Forward-Looking Discussion," *Advanced Materials* 36 (2024): 2406914, https://doi.org/10.1002/adma.202406914.

61. A. P. Deshmukh, W. Zheng, C. Chuang, et al., "Near-Atomic-Resolzution Structure of J-Aggregated Helical Light-Harvesting Nanotubes," *Nature Chemistry* 16 (2024): 800–808, https://doi.org/10.1038/s41557-023-01432-6.

62. X. Chen, I. Weber, and R. W. Harrison, "Hydration Water and Bulk Water in Proteins Have Distinct Properties in Radial Distributions Calculated From 105 Atomic Resolution Crystal Structures," *The Journal of Physical Chemistry B* 112 (2008): 12073–12080, https://doi.org/10.1021/jp802795a.

63. M. L. Ślęczkowski, M. F. J. Mabesoone, P. Ślęczkowski, A. R. A. Palmans, and E. W. Meijer, "Competition Between Chiral Solvents and Chiral Monomers in the Helical Bias of Supramolecular Polymers," *Nature Chemistry* 13 (2021): 200–207.

Supporting Information

Additional supporting information can be found online in the Supporting Information section.

Supporting File: adma72191-sup-0001-SuppMat.pdf.